Spectrochimica Acta Part A: Molecular and Biomolecular Spectroscopy 97 (2012) 1052–1057

Contents lists available at SciVerse ScienceDirect

Spectrochimica Acta Part A: Molecular and Biomolecular Spectroscopy

journal homepage: www.elsevier.com/locate/saa

FTIR spectroscopy study of the structure changes of palygorskite under heating

Wenchang Yan [a,b], Dong Liu [a], Daoyong Tan [a,b], Peng Yuan [a,*], Ming Chen [a]

[a] CAS Key Laboratory of Mineralogy and Metallogeny, Guangzhou Institute of Geochemistry, Chinese Academy of Sciences, Guangzhou 510640, China
[b] Graduate School of Chinese Academy of Sciences, Beijing 100049, China

HIGHLIGHTS

- The assignments of the IR vibrations of palygorskite in the low wavenumber region.
- The structure evolutions of palygorskite during the dehydroxylation process.
- The contributions of the amorphous carbonate and quartz impurities to the IR vibrations.
- The classification of the vibrations of Si–O_1–Si and H_2O–Mg–H_2O.

GRAPHICAL ABSTRACT

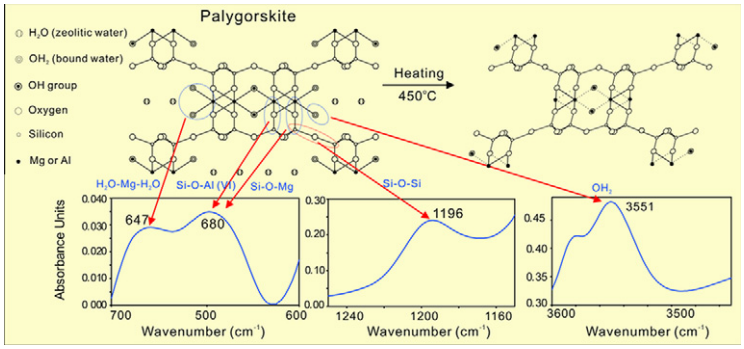

ARTICLE INFO

Article history:
Received 1 February 2012
Received in revised form 27 June 2012
Accepted 11 July 2012
Available online 7 August 2012

Keywords:
Palygorskite
Infrared spectroscopy
Heating
Structure

ABSTRACT

Progressive heat treatment was applied to palygorskite, and the changes of the position and intensity of its infrared vibrations, particularly those in the low wavenumber region, were monitored by use of Fourier transform infrared spectroscopy. Moreover, the responses of the impurities in palygorskite under heating were also examined. Palygorskite is characterized by two bands at 1196 and 647 cm^{-1}, which are attributed to the asymmetric stretching vibration of the Si–O–Si group that connects the adjacent inverse SiO_4 tetrahedrons and the H_2O–Mg–H_2O stretching vibration in the MgO_6 octahedra at the edges of the channels, respectively. The band at approximately 680 cm^{-1} is attributed to the overlapping symmetric stretching vibrations of Si–O–Mg and Si–O–Al (VI). In addition, the 865 cm^{-1} band corresponds to the amorphous carbonate impurity.

Introduction

Palygorskite with an idealized structural formula of $Si_8O_{20}(Al_2Mg_2)(OH)_2{\cdot}(OH_2)_4{\cdot}4H_2O$) [1], which is also called attapulgite in the mining field, is a naturally occurring silicate mineral with a nano-sized fibrous morphology. The structure of palygorskite consists of ribbons of 2:1 phyllosilicate units, and each ribbon is connected to the next by the inversion of SiO_4 tetrahedrons along a set of Si–O–Si bonds, resulting in zeolite-like channels with a size of approximately 0.37 × 0.64 nm. These channels are parallel to the phyllosilicate ribbons and contain zeolitic water and bound water. In the octahedral ribbons of the palygorskite, M1, M2, and M3 octahedral sites exist, as reported by Güven et al. [2]. Al and Fe^{3+} occupy the M2 position, Mg occupies the M1 position, and M3 is vacant (Fig. 1, based on the previous reports [2,3]). In addition, if the Mg/(Al + Fe^{3+}) ratio is >1, M3 position may be partially occupied by Mg. To produce a charge of 10 per half-cell, the most probable distribution of the octahedral cations is that in which the M1, M2, and M3 positions are all occupied by Mg.

Palygorskite has received considerable attention in the fields of adsorption, nanocomposites and catalysis because of its unique crystalline structure as well as its morphological and physic-chemical properties. However, the structure of palygorskite must be

* Corresponding author. Address: Guangzhou Institute of Geochemistry, Chinese Academy of Sciences, Wushan, Guangzhou 510640, China. Tel./fax: +86 20 85290341.
E-mail address: yuanpeng@gig.ac.cn (P. Yuan).

1386-1425/$ - see front matter © 2012 Elsevier B.V. All rights reserved.
http://dx.doi.org/10.1016/j.saa.2012.07.085

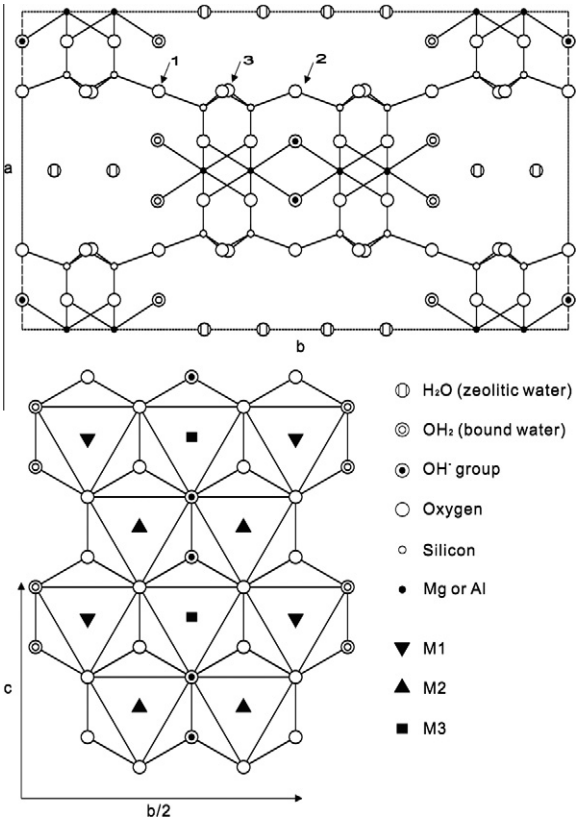

Fig. 1. Palygorskite structure projected on (001) and octahedral ribbon.

further investigated because of its complexity, which is a result of the isomorphic substitution that frequently occurs in tetrahedral and octahedral sheets of palygorskite and the existence of different hydroxyl species in the structure. Fourier transform infrared spectroscopy (FTIR) has been extensively used to investigate the structure of palygorskite, particularly the forms of the hydroxyl species that are relevant to the high wavenumber vibration region. However, a smaller number of studies have focused on developing an in-depth explanation of the low wavenumber region, probably because the related Si–O and M–O vibrations and lattice modes in this region are complicated and difficult to be classified.

In the present work, a progressive heat treatment was applied to palygorskite, and the changes of the position and intensity of its infrared vibrations were monitored with FTIR spectroscopy, particularly the vibrations in the low wavenumber region. Moreover, the responses of the impurities in palygorskite under heating were also examined because most natural palygorskite contains impurities that may provide useful information for enabling a better understanding of the structure of palygorskite. These topics have been largely overlooked in the literature to the best of our knowledge.

Experimental methods

Materials and methods

A raw palygorskite sample from Mingguang, Anhui Province, China, was purified and fractionated by sedimentation. The <5 μm fraction was collected and dried at 60°. The chemical composition (wt.%) of the purified palygorskite (denoted Pal) determined from chemical analysis is as follows: SiO_2, 56.86; Al_2O_3, 10.57; Fe_2O_3, 6.20; MgO, 12.63; CaO, 0.56; Na_2O, 0.05; K_2O, 1.05; MnO, 0.10; TiO_2, 0.99; and L.O.I, 10.76.

The heat treatment of palygorskite was performed in a programmed temperature-controlled muffle oven at scheduled temperatures (200–900 °C) for 1 h. The obtained samples were ground into powder in an agate mortar and are denoted Pal-"*X*", where *X* is the value of the heating temperature.

Characterization and methods

Thermogravimetric (TG) analysis was conducted on a Netzsch STA 449C instrument. Approximately 10 mg of finely ground samples were heated in a corundum crucible from 30 to 1000 °C at a heating rate of 10 °C/min under a highly pure N_2 atmosphere.

The X-ray diffraction (XRD) patterns were measured on a Bruker D8 Advance diffractometer with a Ni filter and CuKa radiation (λ = 0.154 nm) using a generator voltage of 40 kV and a generator current of 40 mA. A scan rate of 1° (2θ)/min was applied for the determination of the XRD patterns.

The FTIR spectra of the samples were recorded on a Bruker Vertex-70 Fourier transform infrared spectrometer at room temperature. The specimens used for measurement were prepared by mixing 0.9 mg of the sample powder with 80 mg of KBr and pressing the mixture into a pellet. Over 64 scans were collected for each sample at a resolution of 4 cm^{-1}.

Results and discussion

XRD

Fig. 2 shows the XRD patterns of Pal and the samples heated at increasing temperature (200–900 °C). The sharp reflections at 8.3, 13.8, 16.4, 19.8, 27.5, and 35.4° (2θ) are attributed to the (110) reflection of palygorskite with the d_{110} spacing of 1.0642 nm, as well as $d_{(200)}$, 0.6486; $d_{(130)}$, 0.5423; $d_{(040)}$, 0.4469; $d_{(240)}$, 0.3675; $d_{(400)}$, 0.3237, and $d_{(161)}$, 0.254 nm. The reflection at approximately 27° (2θ) is attributed to the (101) reflection of quartz, the content (wt.%) of which was semi-quantitatively determined to be approximately 2.2%. The sharp reflection at 20.6° (2θ) with the *d* spacing of 0.4259 nm is attributed to the (100) reflection of quartz. According to the Powder Diffraction File (PDF) of quartz, $I_{(100)} = I_{(101)}{}^{*}22$, but the intensity of the 0.4259 nm reflection was $>I_{(101)}{}^{*}22$. The reflection, therefore, is also contributed by the (121) reflection of palygorskite, which is a characteristic reflection of orthorhombic palygorskite [4], indicating that the sample belongs to be orthorhombic palygorskite.

After heating at 200 and 300 °C, the intensity and position of each reflection of palygorskite remained constant, indicating the stability of the structure. This result meant what has been removed from the Pal mainly was the surface-adsorbed water and zeolitic water.

Remarkable reductions in the intensity of the (110), (400), and (161) reflections were observed in the XRD patterns after heating at 450 and 550 °C. The appearance of the reflection at 9.6° (*d* spacing of 0.912 nm) in Pal-450 and Pal-550 was also observed, which is caused by the dehydration and deformation of the structure [5]. A strong reflection at 20.3° (*d* spacing of 0.435 nm) appeared in Pal-450 and Pal-550. It is a characteristic reflection of monoclinic palygorskite [4], suggesting that the sample is transformed from orthorhombic palygorskite to monoclinic palygorskite. After complete dehydroxylation at 700 °C, the reflection at 9.6 disappeared, indicating that this reflection is related to the structure of palygorskite that appeared after dehydroxylation. However, the (200) reflection still appeared in Pal-700, and the *d* spacing only slightly decreased, which implies the existence of a layered structure. The reflection at 30.1° (*d* spacing of 0.295 nm) appeared in Pal-450, Pal-550, and Pal-700, but not in Pal, Pal-200 and Pal-300; this observation was

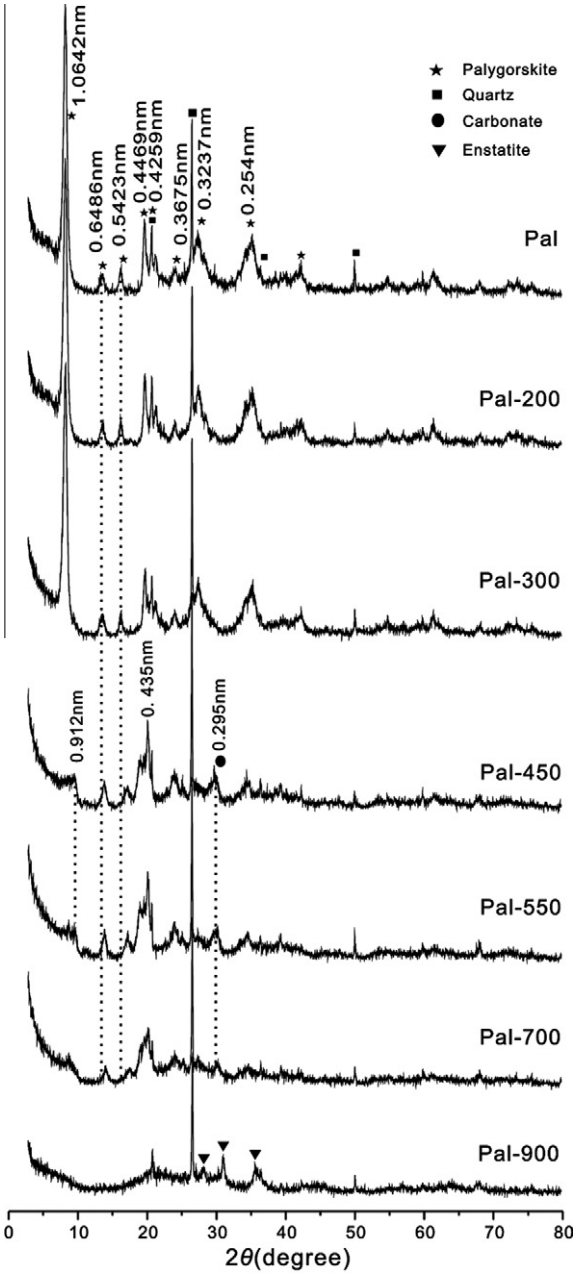

Fig. 2. XRD patterns of Pal and the samples heated at increasing temperature (200–900 °C).

not mentioned in the relevant references [5–7]. Based on the Powder Diffraction File (PDF) database (2004), the 0.295 nm diffraction should be attributed to the carbonate such as $CaMn(CO_3)_2$ and $CaMg(CO_3)_2$, though a more precise assignment is very difficult at this stage. The carbonate is likely sourced from the recrystallization of amorphous carbonate after heating at 450, 550, and 700 °C [8].

All of the previously described reflections of palygorskite disappeared after heating at 900 °C, and the carbonate reflection vanished because of its thermal decomposition. New reflections at 28.1, 31.1, and 35.7° (d spacings of 0.317, 0.287, and 0.252 nm, respectively) appeared after heating at this temperature and are attributed to enstatite. In addition, amorphous SiO_2, which is characterized by the broad diffraction at approximately 22° (2θ) [9], appeared in Pal-900. However, the reflections due to quartz exhibited few changes, indicating that heat treatments up to 900 °C exert few effects on the crystalline structure of quartz.

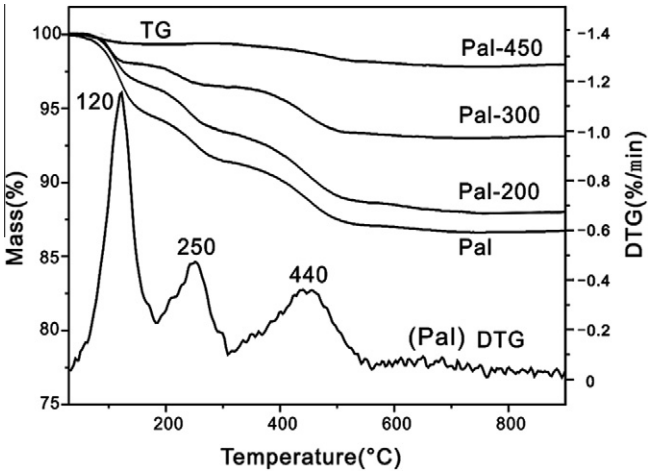

Fig. 3. TG analysis of Pal and the solids produced upon heating at 200, 300 and 450 °C. DTG curve of Pal is also reported.

TG

Three dramatic mass-loss steps appeared at 30–180, 180–300, and 300–600 °C in TG curves, and these steps corresponded to derivative thermogravimetric (DTG) peaks at approximately 120, 250, and 440 °C, respectively (Fig. 3). The first two mass-losses can be attributed to the dehydration of surface-adsorbed water and zeolitic water from the Pal [7]. This result is in good agreement with the XRD results. The last mass loss resulted from the dehydration of tightly bound water and dehydroxylation, during which the structure of Pal was increasingly distorted, but the specimen still kept layer structure based on above XRD results. It is noteworthy that the mass-loss values of the dehydration from 30 to 120 °C differed slightly between Pal, Pal-200, and Pal-300, and they differed significantly for Pal-450. This difference may be due to the rapid re-adsorption of water on the surface and in pores during measurement procedure after heating at $\leqslant$300 °C; Nevertheless, the re-adsorption of water became more difficult after the dehydration of bound water at 450 °C because some modifications of the internal surfaces of the channel and the external surfaces of Pal occur at this condition.

FTIR spectroscopy

The high wavenumber region (4000–1500 cm^{-1})

Fig. 4 shows the FTIR spectra of the high wavenumber region of Pal and the solids heated at increasing temperature and the corresponding wavenumbers of the main vibrational bands are identified. Among them, two shoulder bands at approximately 3686 and 3580 cm^{-1}, as well as a sharp band at approximately 3616 cm^{-1}, are attributed to the stretching vibrations of Mg_3–OH, Al–OH–Fe^{3+}, and Al–OH–Al, respectively [10,11]. These bands disappeared after heating at 700 °C because of the complete dehydroxylation, as described in the XRD and TG analysis sections.

The characteristic FTIR band at approximately 3551 cm^{-1} is attributed to the stretching vibration of bound water in Pal [11]. It shifted to 3525 cm^{-1} after heating at 450 and 550 °C, at which points the structure distorted, the porous channels become blocked, and a few bound water molecules in the channels still existed. The residual bound water molecules were removed at 700 °C. The band at approximately 3403 cm^{-1} is attributed to the stretching vibration of water molecules, including zeolitic water and surface-adsorbed water in Pal. The band at 3431 cm^{-1} appeared after heating at 450 °C because of the re-adsorption of water during the experimental procedure.

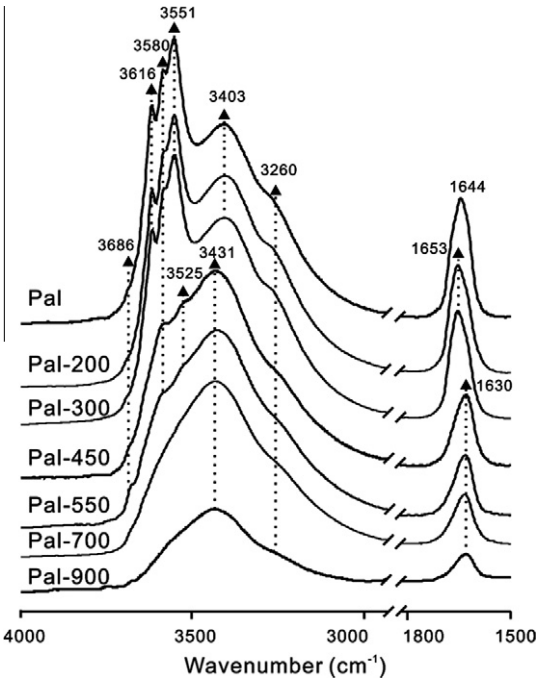

Fig. 4. FTIR spectra of Pal and the solids heated at increasing temperature (200–900 °C). Spectra are reported in the 4000–1500 cm^{-1} range.

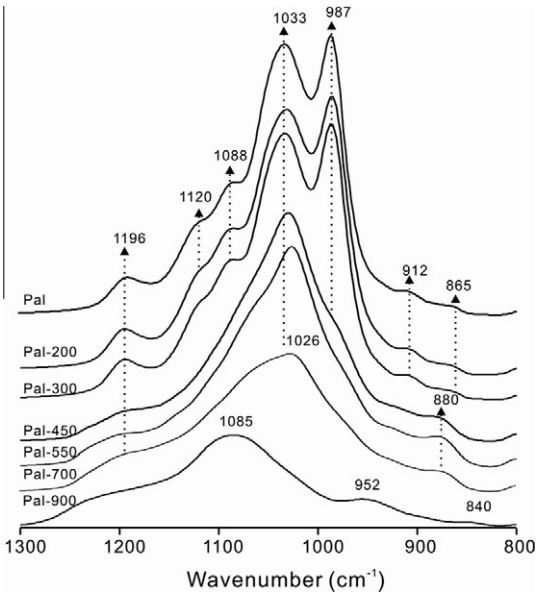

Fig. 5. FTIR spectra of Pal and the solids heated at increasing temperature (200–900 °C). Spectra are reported in the 1300–800 cm^{-1} range.

An asymmetric band centered at 1644 cm^{-1} in the sample, which corresponds to the bending modes of the above-mentioned water molecules, can be resolved into two bands at approximately 1660 and 1630 cm^{-1}, which are attributed to the bound water and adsorbed water, respectively [12]. After heating the samples at 300 °C, the band shifted to 1653 cm^{-1} which is attributable to the bound water because most of the zeolitic and surface-adsorbed water has been removed. While complete dehydration and dehydroxylation occurred at 700 °C, the band at approximately 1630 cm^{-1} still appeared, indicating that the band results from the re-adsorbed water.

The low wavenumber region (1300–400 cm^{-1})

Fig. 5 shows the FTIR spectra of 1300–800 cm^{-1} of Pal and the solids heated at increasing temperature. The Si–O vibration bands of palygorskite are displayed in the FTIR spectra of the wavenumber range of 1200–950 cm^{-1} and assigned to Si–O–M (VI), Si–O–Si, and SiO_4 tetrahedral base breathing vibrations. Five characteristic bands appeared at 987, 1033, 1088, 1120, and1196 cm^{-1} in the corresponding region of Pal. The 987 cm^{-1} band is attributed to the perpendicular Si–nonbridging oxygen–Mg (Si–O_{nb}–Mg) asymmetric stretching vibration based on a previous report [13].

The assignment of the band at approximately 1088 cm^{-1} was controversial, and it was usually regarded as the vibration of Si–O–Si or SiO_4 tetrahedron base breathing [13]. However, considering the existence of this band in many nesosilicate minerals that lack Si–O–Si bonds, such as almandine and grossular [14], the band should be attributed to SiO_4 tetrahedron base breathing stretching vibration. The additional evidence that the band disappeared after heating at 450 °C because of the distortion of the tetrahedral sheet gives strong support to this proposal.

There exist three types of Si–O–Si (Si–bridging oxygen–Si) bonds in palygorskite: the first (denoted Si–O_1–Si) connects the two inverse SiO_4 tetrahedrons (labeled as 1 in Fig. 1), the second (denoted Si–O_2–Si) connects two SiO_4 tetrahedrons in the two pyroxene chains (labeled as 2 in Fig. 1), and the third (denoted Si–O_3–Si) connects the two SiO_4 tetrahedrons in a single pyroxene chain (labeled as 3 in Fig. 1). The bond angles decrease in the following order: Si–O_1–Si (approximately 180°) > Si–O_2–Si > Si–O_3–Si [13]. The larger bond angle of Si–O_2–Si is caused by the angular distortion of the SiO_4 tetrahedrons required to match the AlO_6 octahedra that occupy the M2 position, showing dioctahedral characteristic of palygorskite.

The three bands at 1196, 1120 and 1033 cm^{-1} are assigned to the asymmetric stretching vibrations of the Si–O_1–Si, Si–O_2–Si, and Si–O_3–Si bonds, respectively, because the wavenumber of the corresponding IR band increases with the increment of the bond angle for the same type of bond. The band at approximately 1196 cm^{-1} also appears in minerals with Si–O–Si bonds connecting two inverse SiO_4 tetrahedrons (as in palygorskite), such as sepiolite, antigorite and cristobalite [14]. The intensity of the Si–O_1–Si band gradually decreased after heating at 450–700 °C, but it still appeared as a shoulder band, which indicates the existence of a layered structure despite the decreased ordering degree of the palygorskite. This result is in good agreement with the XRD results. The Si–O_1–Si band disappeared at 900 °C because of the phase transition. The 1120 cm^{-1} band related to the dioctahedral characteristic of palygorskite [11] remained constant after heating at ⩽300 °C and disappeared at 450 °C. However, the 1033 cm^{-1} band shifted slightly toward low wavenumbers at 450 and 550 °C and did not disappear until heating at 900 °C.

The band at approximately 910 cm^{-1}, which is assigned to the bending vibration of Al–OH–Al [10,11], disappeared after heating at 450 °C because of the dehydroxylation of Al–OH–Al.

A shoulder band centered at approximately 865 cm^{-1} was attributed to the bending vibration mode of the Al–OH–Fe bond of palygorskite by Chahi et al. [12]. However, in some references, the band did not appear even though the Al-OH-Fe^{3+} bond existed [1,10,13], implying that the assignment of this band was controversial. Dupuis et al. assigned the 865 cm^{-1} band to the CO_3^{2-} bending vibration of amorphous carbonate [15]. In this study, the 865 cm^{-1} band disappeared after heating at 450 °C, and two new bands at approximately 880 and 748 cm^{-1} (due to carbonate) [16] appeared simultaneously. This phenomenon implies that the 865 cm^{-1} band corresponds to amorphous carbonate, which is transformed into crystalline carbonate at 450 °C. This result provides strong support to the above-mentioned XRD results. The

two carbonate bands disappeared at 900 °C because of thermal decomposition.

Fig. 6 shows the FTIR spectra of 800–400 cm^{-1} of Pal and the solids heated at increasing temperature. In this region, the Si–O–M–O–M bonds are very complex, and there are few references regarding this FTIR region in palygorskite. Two bands at approximately 798 and 781 cm^{-1} are present, and they have been previously described as the Si–O–Si symmetric stretching vibration of quartz only. However, the intensity and position of the band changed after heating at 900 °C, indicating that the Si–O–Si structure was partially destroyed. Nevertheless, the previous XRD result shows that few alterations of the quartz structure existed after calcination at 900 °C. In this case, the two bands are attributed to the overlapping of the Si–O–Si vibrations of quartz and palygorskite, and the change of the bands at 900 °C is caused by the disappearance of the above-mentioned Si–O–Si band (1033 cm^{-1}) of palygorskite because of the complete destruction of the palygorskite structure.

There existed a weak, broad, and asymmetric band centered at 680 cm^{-1}. This band was resolved into two bands after heating at 450 °C, which appeared at 672 (as a shoulder) and 692 cm^{-1}. The former band is proposed to be related to the Mg content [11], and it is attributed to the Si–O–Mg symmetric stretching vibration. The latter band, which universally appears in dioctahedral minerals, such as kaolinite and halloysite, is attributed to the symmetric stretching vibration of the characteristic Si–O–Al (VI) [17]. Because of the influence of the MgO_6 octahedrons adjacent to the AlO_6 octahedron, the corresponding wavenumber of the Si–O–Al (VI) vibration band shifted to the low region (685 cm^{-1}) of the IR spectra of Pal. In contrast, the Si–O–Mg band shifted to the high region. After heating at 450 °C, the MgO_6 octahedra at the edges of the channels were destroyed due to the removal of bound water, and the characteristic Si–O–Al vibration of the dioctahedron appeared at ~692 cm^{-1}. In this case, the broad band at 680 cm^{-1} in the IR spectra of Pal is attributed to the overlapping vibrations of Si–O–Mg and Si–O–Al (VI).

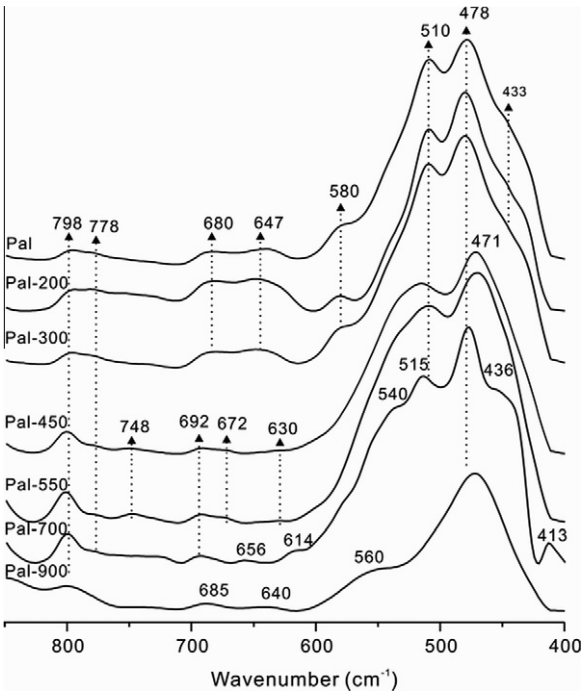

Fig. 6. FTIR spectra of Pal and the solids heated at increasing temperature (200–900 °C). Spectra are reported in the 800–400 cm^{-1} range.

The band at approximately 647 cm^{-1} in palygorskite and sepiolite does not appear in other phyllosilicates such as talc, montmorillonite, and illite [14], indicating that the band might be a characteristic vibration of palygorskite and have relation with the particular channel structure. Tarte et al. attributed it to the symmetric stretching vibration of Si–O_1–Si which connects the two inverse SiO_4 tetrahedrons [18]. The band at 647 cm^{-1} in Pal-450 almost disappeared, but the 1196 cm^{-1} (the Si–O_1–Si asymmetric stretching vibration) only decreased its intensity. Moreover, the Si–O_1–Si symmetric stretching vibration should be with higher wavenumber than that of the Si–O_3–Si vibration, while the bands at approximately 798 and 781 cm^{-1} have been previously described as the Si–O_3–Si symmetric stretching vibration. Therefore, the assignment of 647 cm^{-1} band to the Si–O_1–Si vibration was questionable. McKeown et al., based on the lattice dynamic calculation, confirmed that the band should be related to the O–Mg–O stretching vibration in palygorskite and sepiolite [13], which have similar structures and both have bound water. However, the band does not appear in talc, which consists of MgO_6 octahedrons but has no bound water, indicating that the band should be attributed to the unique O–Mg–O vibration. In addition, McKeown et al. did not distinguish the O–Mg–O and H_2O–Mg–H_2O force constant values calculated for palygorskite, and the band disappeared after the removal of bound water at 450 °C. The band, therefore, should be attributed to the H_2O–Mg–H_2O stretching vibration.

Four new bands at 656, 614, 436, and 414 cm^{-1} which appear universally in nesosilicate minerals (such as azorite and forsterite), occurred in Pal-700 and are attributed to the Si–O vibration [19,20]. This result indicates that the SiO_4 tetrahedral ribbons of palygorskite have been partially broken down after heating at 700 °C. Another four new bands at 952, 840, 640, and 560 cm^{-1} appeared in Pal-900. These bands are assigned to enstatite by Victoria E. Hamilton [21]. This is good agreement to the XRD result.

The two bands at 580 and 433 cm^{-1} should be attributed to the AlO_6 and MgO_6 octahedron stretching vibrations, respectively [22], and appeared as very weak bands after heating at 450 °C because of dehydroxylation.

The band at approximately 510 cm^{-1} in Pal was attributed to silicate tetrahedral sheet deformation and Si–O–Si bending vibration [13]. It was resolved into two bands at approximately 515

Table 1
Positions and assignments of the infrared vibration bands.

Position (cm^{-1})	Assignments	Position (cm^{-1})	Assignments
433	[a]V_s, MgO_6 octahedron	1088	V_{as}, SiO_4 tetrahedral base breathing
478	[b]δ, O–Si–O	1120	V_{as}, Si–O_2–Si
510	δ, Si–O–Si; silicate tetrahedral sheet deformation	1196	V_{as}, Si–O_1–Si
580	V_s, AlO_6 octahedron	1630	δ, H_2O
647	V_s, [c]H_2O–Mg–H_2O	1653	δ, [e]OH_2
672	V_s, Si–O–Mg	3260	V_s, H_2O bound to oxygen in Si–O–Al(IV) [23]
692	V_s, Si–O–Al	3403–3431	V_s, H_2O
778/798	SiO_2; V_s, Si–O_2–Si	3551/3525	V_s, OH_2
910	δ, Al–OH–Al	3580	V_s, Al–OH–Fe^{3+}
987	[d]V_{as}, Perpendicular Si–O_{nb}–Mg(VI)	3615	V_s, Al–OH–Al
1033	V_{as}, Si–O_3–Si	3686	V_s, Mg_3–OH

[a] V_s Symmetric stretching vibration.
[b] δ Bending vibration.
[c] H_2O Zeolitic and surface-adsorbed water.
[d] V_{as} Asymmetric stretching vibration.
[e] OH_2 Bound water.

and 540 cm^{-1} after heating at 450 °C because of the deformation of the palygorskite structure. The band existed after heating at 700 °C and disappeared at 900 °C, which is in agreement with the change of the 1033 cm^{-1} band related to the stability of the SiO_4 tetrahedral sheet.

The strong band at approximately 478 cm^{-1} appeared in Pal and its heated products, which contained its phase transition product (enstatite). This phenomenon indicates that the vibration is independent of the structure of palygorskite. In this case, it should be attributed to the O–Si–O bending mode of the SiO_4 tetrahedron, which is not disturbed by heating. (see Table 1).

Conclusion

Heat treatments with temperatures up to 900 °C lead to dramatic changes in the crystalline structure of palygorskite. FTIR characterization demonstrates that most of the hydroxyls of palygorskite are removed at approximately 450 °C and that the dehydroxylation is complete at approximately 700 °C, resulting in that the production of SiO_4 tetrahedral sheets become increasingly disconnected but retain a layered structure.

Moreover, some assignments of the IR bands in the low wavenumber region are proposed based on the position and intensity changes of the infrared vibrations of palygorskite. The 865 cm^{-1} band corresponds to the amorphous carbonate impurity, and the bands at 798 and 778 cm^{-1} should be partially attributed to the $Si–O_3–Si$ bond of palygorskite, rather than completely attributed to the quartz impurity. The characteristic 1196 and 647 cm^{-1} bands of palygorskite are assigned to the asymmetric stretching vibration of the $Si–O_1–Si$ that connects the adjacent inverse SiO_4 tetrahedrons and the $H_2O–Mg–H_2O$ stretching vibration in MgO_6 octahedrons at the edges of the channels, respectively. In addition, the IR bands at 692 and 672 cm^{-1} are attributed to the perpendicular Si–O–Al stretching and Si–O–Mg stretching, respectively. These fundamental results are significant to the understanding of the structural evolution of palygorskite under heating as well as to the structure-based applications of palygorskite.

Acknowledgements

This work is financially supported by the Knowledge Innovation Program of the Chinese Academy of Sciences (Grant No. KZCX2-YW-QN101) and the National Natural Science Foundation of China (Grant No. 41072032). This is a contribution (No. IS1528) from GIGCAS.

References

[1] E. Garcia-Romero, M.S. Barrios, M.A.B. Revuelta, Clay Clay Miner. 52 (2004) 484–494.
[2] N. Güven, J.B.D. Delacaillerie, J.J. Fripiat, Clay Clay Miner. 40 (1992) 457–461.
[3] W.F. Bradley, Am. Mineral. 25 (1940) 405–410.
[4] J. Chisholm, Can. Mineral. 30 (1992) 61–73.
[5] H. Hayashi, R. Otsuka, N. Imai, Am. Mineral. 54 (1969) 1613–1617.
[6] E.G. Vanscoyoc, J.C. Serna, L.J. Ahlrichs, Am. Mineral. 64 (1979) 215–223.
[7] N. Frini-Srasra, E. Srasra, Surf. Eng. Appl. Elect+. 44 (2008) 43–49.
[8] N. Koga, Y. Nakagoe, H. Tanaka, Thermochim. Acta 318 (1998) 239–244.
[9] P. Yuan, D. Yang, Z. Lin, H. He, X. Wen, L. Wang, F. Deng, J. Non-Cryst. solids 352 (2006) 3762–3771.
[10] A. Chahi, S. Petit, A. Decarreau, Clay Clay Miner. 50 (2002) 306–313.
[11] M. Suarez, E. Garcia-Romero, Appl. Clay Sci. 31 (2006) 154–163.
[12] R.L. Frost, G.A. Cash, J.T. Kloprogge, Vib. Spectrosc. 16 (1998) 173–184.
[13] D.A. McKeown, J.E. Post, E.S. Etz, Clay Clay Miner. 50 (2002) 667–680.
[14] M.J. Wilson, Clay Mineralogy: Spectroscopic and Chemical Determinative Methods, Chapman & Hall Oxford, London, 1994.
[15] T. Dupuis, J. Ducloux, P. Butel, D. Nahon, Clay Miner. 19 (1984) 605–614.
[16] J.F. Balascio, W.B. White, J. Cryst. Growth 23 (1974) 101–104.
[17] H. Van der Marel, H. Beutelspacher, Atlas of Infrared Spectroscopy of Clay Minerals and their Admixtures, Elsevier Scientific, Amsterdam, 1976.
[18] P. Tarte, J. Preudhom, Spectrochim. Acta A 29 (1973) 1301–1312.
[19] P. Dawson, Mm. Hargreav, Gr. Wilkinso, J. Phys. Part C 4 (1971) 240–246.
[20] R.G. Burns, F.E. Huggins, Am. Mineral. 57 (1972) 967–969.
[21] V.E. Hamilton, J. Geophys. Res.-Planet 105 (2000) 9701–9716.
[22] A.S. Povarennykh, Mineral. Mag. 42 (1978) 518–519.
[23] C. Blanco, J. Herrero, S. Mendioroz, J.A. Pajares, Clay Clay Miner. 36 (1988) 364–368.